TISSUE ENGINEERING: Part A
Volume 20, Numbers 15 and 16, 2014
© Mary Ann Liebert, Inc.
DOI: 10.1089/ten.tea.2013.0455

Synergistic Effects of Matrix Nanotopography and Stiffness on Vascular Smooth Muscle Cell Function

Somali Chaterji, PhD,[1] Peter Kim, BS,[2] Seung H. Choe,[1] Jonathan H. Tsui, MS,[2] Christoffer H. Lam,[1] Derek S. Ho, BS,[1] Aaron B. Baker, PhD,[1] and Deok-Ho Kim, PhD[2–4]

Vascular smooth muscle cells (vSMCs) retain the ability to undergo modulation in their phenotypic continuum, ranging from a mature contractile state to a proliferative, secretory state. vSMC differentiation is modulated by a complex array of microenvironmental cues, which include the biochemical milieu of the cells and the architecture and stiffness of the extracellular matrix. In this study, we demonstrate that by using UV-assisted capillary force lithography (CFL) to engineer a polyurethane substratum of defined nanotopography and stiffness, we can facilitate the differentiation of cultured vSMCs, reduce their inflammatory signature, and potentially promote the optimal functioning of the vSMC contractile and cytoskeletal machinery. Specifically, we found that the combination of medial tissue-like stiffness (11 MPa) and anisotropic nanotopography (ridge width_groove width_ridge height of 800_800_600 nm) resulted in significant upregulation of calponin, desmin, and smoothelin, in addition to the downregulation of intercellular adhesion molecule-1, tissue factor, interleukin-6, and monocyte chemoattractant protein-1. Further, our results allude to the mechanistic role of the RhoA/ROCK pathway and caveolin-1 in altered cellular mechanotransduction pathways via differential matrix nanotopography and stiffness. Notably, the nanopatterning of the stiffer substrata (1.1 GPa) resulted in the significant upregulation of RhoA, ROCK1, and ROCK2. This indicates that nanopatterning an 800_800_600 nm pattern on a stiff substratum may trigger the mechanical plasticity of vSMCs resulting in a hypercontractile vSMC phenotype, as observed in diabetes or hypertension. Given that matrix stiffness is an independent risk factor for cardiovascular disease and that CFL can create different matrix nanotopographic patterns with high pattern fidelity, we are poised to create a combinatorial library of arterial test beds, whether they are healthy, diseased, injured, or aged. Such high-throughput testing environments will pave the way for the evolution of the next generation of vascular scaffolds that can effectively crosstalk with the scaffold microenvironment and result in improved clinical outcomes.

Introduction

Vascular smooth muscle cells (vSMCs) regulate the vasomotor tone of blood vessels by virtue of their contractile function. However, given the need for long-term adaptation through structural remodeling in pregnancy, exercise, or vascular injury, vSMCs retain the ability to undergo modulation in their phenotypic continuum. This continuum ranges from a mature contractile state to a proliferative, secretory state; these states differ in the expression of vSMC-restricted contractile protein genes, which strikingly contain the conserved CArG box DNA sequences within their promoters.[1–3] vSMC differentiation is modulated by a complex array of microenvironmental cues, which include the biochemical milieu of the cells and the architecture and stiffness of the extracellular matrix (ECM). It is known that ECM proteins such as elastin and collagen, comprising the bulk of the ECM of the tunica media, present a nanoscale architecture,[4] that can potentially control the polarization of vSMCs in the artery. While there is some debate on the specific orientation of vSMCs in the arterial wall,[5] it is clear that vSMCs and the ECM collagen and elastin have a directional organization.[6] Nano-sized features are known to topographically regulate the anisotropy of resident cells, regulating cell polarization, cytoskeletal alignment,[7] and even altering the nuclear architecture.[8] This is in stark contrast to the randomness in orientation presented by vSMCs cultured on traditional tissue culture

[1]Department of Biomedical Engineering, Cockrell School of Engineering, The University of Texas at Austin, Austin, Texas.
[2]Department of Bioengineering, University of Washington, Seattle, Washington.
[3]Center for Cardiovascular Biology, University of Washington, Seattle, Washington.
[4]Institute for Stem Cell and Regenerative Medicine, University of Washington, Seattle, Washington.

substrata. Thus, the rationale for nanopatterning the soft and stiff substrata was borne out of the desire to enhance the biomimetic properties of the substrata, specifically to mimic the topography of the native basement membrane.[7,9,10]

Surface topographies have been demonstrated to have an effect in a wide range of mammalian cells, tabulated in Bettinger *et al.*[11] This is because cells themselves are known to form focal adhesions, which are in the 1–10 μm range,[12] with nascent focal adhesions involved in complex mechanical interactions, being significantly smaller.[13,14] Thus, feature sizes on substrata that are commensurate with the size of these focal complexes can potentially evoke cell–substrata adhesive signals of the desired condition of the engineered tissue, be it healthy, diseased, aging, or post-injury remodeling tissue. Contact guidance describes the phenomenon by which cells recognize and respond to altered extracellular topography by changing their morphology, orientation, and behavior, resulting in altered signaling events. In fact, it has been demonstrated in our previous studies that optimal contact guidance, modulated by the substratum's engineered architecture, resulted in focal adhesion formation predominantly at the cell-groove interface of the topographical ridges,[15] which could be useful in engineering myocardial tissue.[16]

Our prior work has demonstrated our ability to fabricate nanotopographically controlled systems with high fidelity. Of specific relevance to this work are anisotropically-nanofabricated substrata (ANFS), as opposed to randomly oriented nanoscale cues, which afford anisotropic nanotopographic stimuli for modulating cell signaling and function.[15,17,18] The ability to design and fabricate synthetic tissue scaffolds that can recapitulate the multiscale cell–matrix connections *in vivo* can (i) result in more biomimetic constructs for tissue repair and reconstruction, and (ii) create testbeds to perform molecular engineering and testing in more physiologically relevant platforms. This ability to alter the nanotopography of the fabricated surfaces, coupled with the integration of these surfaces with conventional multi-well plates, as in the current study, or in microfluidic platforms,[19–21] serves as an enabling tool for the development of nanolithography-based devices for multiscale, multiple-input, spatial control of cell homeostasis and function. While probing the ability of cells to respond to contact guidance has gained traction,[15,17,22] the mechanisms and pathophysiological consequences of such cues in various cell types are still under scrutiny. It is well recognized, however, that by adding nanoscale topography to 2D substrata, one can recreate some of the complexity of 3D microenvironments while retaining the convenience of working in 2D.

To make the combinatorial testing of cell function robust in this study, we have simultaneously altered the stiffness of the nanopatterned polymeric substrata to mimic the stiffness of soft tissue. In cellular mechanotransduction studies, polyacrylamide and gelatin gels have been widely used to alter the stiffness of the substratum.[23] However, it has been noted in the literature that the elastic moduli and interfacial tension of the substratum set the resolution limit for molding well-defined microscale structures with the complexity of native tissues.[24] Thus, our goal was to imprint anisotropic topographic features of the nanometer scale with high fidelity on mechanically compliant biocompatible surfaces. With this in mind, we designed and fabricated polyurethane (PU)-based ANFS of 800_800_600 nm (ridge width_groove width_ridge height) pattern and of differential stiffness, specifically, one with a healthy medial tissue-like elastic modulus of 11 MPa[25] and, another, with a higher elastic modulus of 1.1 GPa to study the synergistic effects of substratum nanotopography and stiffness on vSMC behavior. We fabricated control unpatterned (topographically flat) substrata and nanopatterned surfaces, and examined vSMC behavior on these engineered surfaces. Specifically, we were interested in studying (i) the differentiation state of the vSMCs driven by altered transcription of vSMC-restricted contractile protein genes,[2] (ii) the activation state of the cells using markers known to be upregulated in atherosclerosis,[26] and (iii) the actin cytoskeletal changes potentially driving the mechanical plasticity of vSMCs.[27]

The results presented in this study point to our ability to mimic native matrix microenvironments while deconstructing the complexity of the cellular extracellular matrices. Using a novel nanofabrication technology gaining traction in regenerative medicine, namely, UV-assisted capillary force lithography (CFL), we fabricated ANFS of different stiffnesses. We then cultured a monolayer of vSMCs to form a complete smooth muscle layer and found that vSMC phenotypic modulation was regulated by the nanotopography of the substrata, and that nanopatterning the substrata also attenuated inflammatory gene expression. Importantly, we mimicked the smooth muscle layers present *in vivo* by ensuring the completeness of the cultured vSMC layer prior to conducting downstream studies. Since cell–cell interactions exert a strong influence on cell morphology in a substratum stiffness-dependent manner,[28] it is possible that effects of the differences in substrata would be more dramatic in vSMCs in a sub-confluent muscle layer. However, since our goal was to study the effect of micromechanical properties of the substrata in an *in vivo*-like setting, our studies were carried out in the presence of extensive cell–cell contacts and, essentially, modulated by the cell-deposited ECM.[29]

Materials and Methods

Fabrication of the poly(urethane acrylate) mold

Silicon wafers with 800_800 nm nanogroove features were fabricated by a micro-stamping method as described in Kim *et al.*[17] Briefly, this involved spin-coating the silicon wafers with a photoresist (Shipley), patterning via electron-beam lithography (JBX-9300FS, JEOL), photoresist development (MF320, Shipley) and deep reactive ion etching of exposed silicon, removal of the remaining photoresist, and finally, dicing into silicon masters for subsequent replica molding. These etched features on the silicon masters were then transferred to poly(urethane acrylate) (PUA) molds (~50 μm thickness) on polyester film for the fabrication of nanopatterned PUA substrata by a UV-assisted nanomolding method used previously[17,18] (Fig. 1A).

Fabrication of unpatterned and nanopatterned PUA substrata using UV-assisted CFL

Glass coverslips were first rinsed in isopropyl alcohol in a sonicated bath at 35°C for 20 min and blow-dried. The coverslips were then oxygen-plasma treated for 5 min. Adhesion promoter (Minuta) was applied to the glass coverslips by

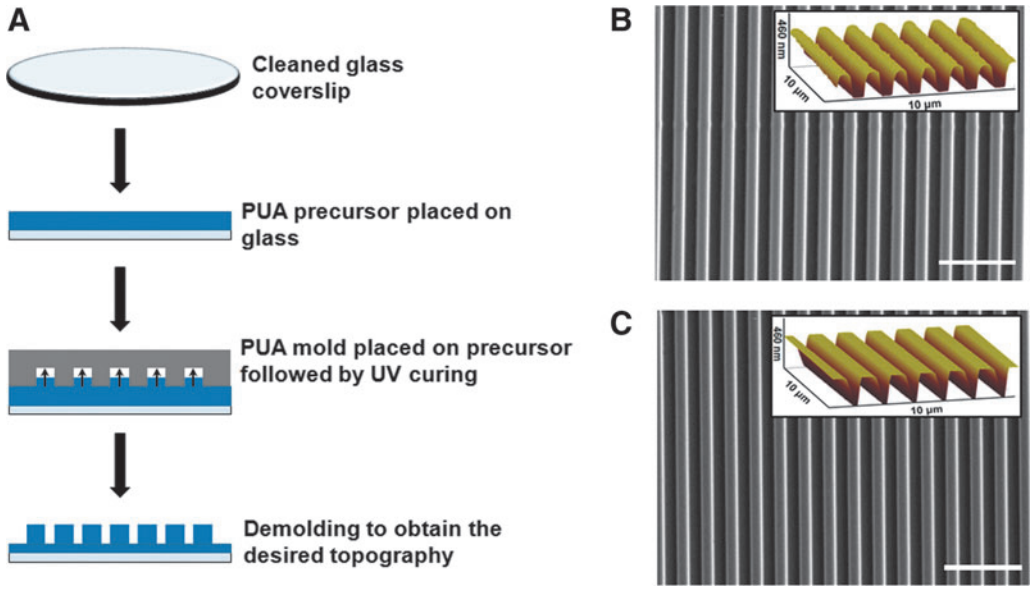

FIG. 1. Fabrication and characterization of large-area, anisotropically-nanofabricated substrata (ANFS). **(A)** Schematic for UV-assisted capillary force lithography (CFL) used to fabricate nanopatterned substrata. Scanning electron microscope image with atomic force microscope image inset demonstrating the generation of nanogrooves using the method on **(B)** 11 MPa (NOA73) substrata and **(C)** 1.1 GPa (NOA83H) substrata. Substrata of both stiffnesses featured the same topographical dimensions of 800_800_600 nm (ridge width_groove width_ridge height). Scale bars: 5 µm. PUA, poly(urethane acrylate).

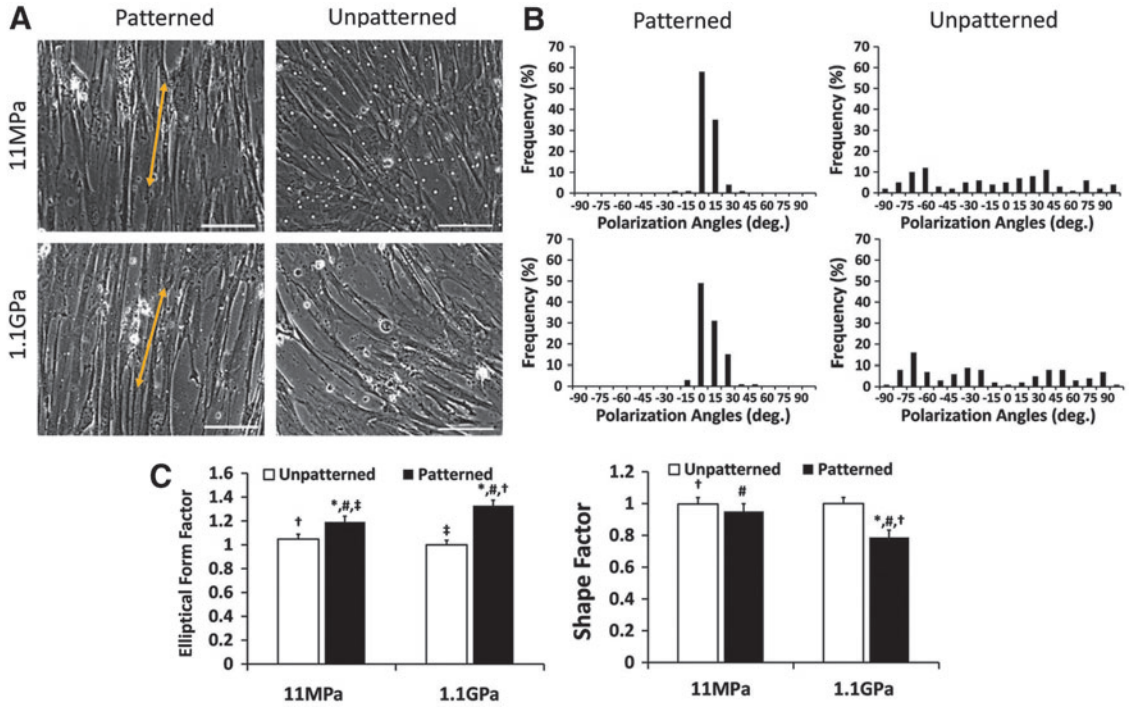

FIG. 2. Morphology and orientation of human umbilical artery smooth muscle cells on engineered substrata. **(A)** Representative images demonstrating the morphology and orientation of the cells cultured and differentiated using smooth muscle differentiation supplement (SMDS)-supplemented vascular smooth muscle cell (vSMC) culture medium on different substrata, unpatterned or ANFS. Scale bar: 20 µm. **(B)** Depictions of cell orientation on the unpatterned and nanopatterned surfaces, the cells are clearly more directionally polarized on ANFS. $n = 100$ (cells) for each condition. Statistically significant difference between nanopatterned and unpatterned substrata ($p < 0.05$) for the same substratum stiffness is indicated with an asterisk. For all other substrata-type combinations, the identical signage indicates statistically significant difference for that pair. **(C)** Elliptical form factor (EFF) determinations indicated that vSMCs on unpatterned substrata were shorter and wider than the vSMCs cultured on ANFS; shape factor determinations indicated that the vSMCs on the stiffer ANFS were less circular than on the softer ANFS ($p < 0.05$).

spin-coating at 2000 rpm for 20 s. Once spin-coated, the coverslips were baked at 65°C for 20 min. Then PUA-based polymers of commercially characterized stiffness, 11 MPa (NOA73) and 1.1 GPa (NOA83H) (Norland Products, Inc.), were drop dispensed on the coverslips. Nanopatterned NOA substrata of higher and lower stiffnesses were fabricated from the PUA copy of the nanogroove features. The patterns were UV cured using a wavelength of 365 nm for 60 s. After polymerization, the PUA nanogrooved master was removed. The substrata were then exposed to UV overnight for sterilization and to complete the curing process. This resulted in the formation of ANFS. Unpatterned surfaces were fabricated from flat polyester films instead of the PUA copy of the nanogrooved surface. These substrata were then glued to multi-well plates (MatTek Corp) for cell culture and analyses.

Scanning electron microscopy

For examining and verifying the topography of the ANFS, samples were sputter-coated with an $\sim$10 nm thick layer of Au/Pd alloy and were imaged with an accelerating voltage of 5 kV using a scanning electron microscope (SEM; Sirion, FEI). Both top-view and cross-sectional SEM images were taken.

Atomic force microscopy

The ANFS features were also examined using an atomic force microscope (AFM, Dimension 3100; Veeco) in tapping mode with a NanoProbe OTESPA (Silicon) tip. Analysis was conducted with an AS-12VMF (EV) scanner with a lateral (X-Y) range of 10×10 μm and a vertical (Z) range of 2.5 μm. The images were obtained with a scan rate of 0.996 Hz and a sampling resolution of 512 lines $\times$ 512 pixels per line. The best resolution was acquired by setting the peak amplitude to 1.541 V and by modulating the proportional and integral gains to 0.400 and 0.200, respectively.

Cell culture, seeding, and stimulation of vSMC differentiation

Human umbilical artery smooth muscle cells (#CC-2579; Lonza) were maintained in MCDB-131 media supplemented with 10% fetal bovine serum (FBS), 1% penicillin/streptomycin, and 1% L-glutamine. Prior to seeding cells, the substrata were incubated overnight in complete (10%) serum medium to deposit a layer of blood proteins as would happen after the deployment of a vascular device or implant. Next, seeding of a near-confluent density of cells was done and then allowed to get fully confluent and kept for another 24 h to facilitate the formation of an *in situ* generated ECM.[29] This was done to more closely replicate the functionality of a vascular smooth muscle layer. For differentiation of vSMCs, differentiation media containing a smooth muscle differentiation supplement (SMDS) comprising of 1% FBS and 30 μg/mL heparin (heparin sodium; Sigma) was used. All media supplements were obtained from Life Technologies, unless otherwise specified. All downstream analyses were done 48 h after the addition of the differentiation treatments to ensure sample to sample reproducibility and to allow enough time for the altered transcription of differentiation-related genes in vSMCs as a result of the treatment.

Cell alignment and cell shape analysis

For determination of alignment and morphology, cells were treated with the differentiation media and cultured for 2 days on the different substrata prior to imaging. A minimum of 10 randomly selected areas (10$\times$ objective, Zeiss Axio Observer fluorescence microscope) in 10 images for each group were analyzed. Analysis was done via computer-assisted morphometry (Metamorph 7.0; Molecular Devices) or ImageJ. Measurements were made of the elliptical form factor (EFF; defined as the major axis divided by minor axis) and shape factor (defined as $4\pi A/P^2$, where P is the perimeter and A is the area of the cell). This was done to check whether the nanopatterning resulted in more directionally polarized and elongated cells. In addition, cell alignment was measured using ImageJ, with the direction of the nanogrooves as the reference frame, which was set as the y-axis. With the freehand selections mode, the cells were circled and then analyzed using the analyze tool in ImageJ. Excel was used to analyze the exported data and then generate the cell alignment histograms.

Immunocytochemical staining for F-actin stress fibers

For determination of cytoskeletal orientation, cells were seeded at densities of 8×10^4 cells/cm^2 and maintained in a proliferative medium. Confluent cultures were differentiated using SMDS-containing differentiation medium. Forty-eight hours after culture, cultures were washed with phosphate-buffered saline (PBS), fixed with 4% paraformaldehyde for 20 min, followed by permeabilization with 0.2% Triton-X for $\sim$10 min at room temperature. The cultures were then blocked with 5% FBS in PBS for 1 h at room temperature. Alexa Fluor 594-labeled phalloidin conjugate was used for staining F-actin stress fibers. After extensive PBS washes, the cultures were mounted in antifade medium (Vector Labs) and imaged using a Zeiss fluorescent microscope. Next, quantitative analysis of F-actin stress fiber alignment was performed by using the gradient orientation approach implemented in Matlab (Mathworks) as previously described in Cho *et al.*[30] Briefly, for pixel gradient analysis, Gaussian low pass filter and Sobel horizontal edge-emphasize filter (predefined in Matlab Image Analysis Toolbox) were used to implement a two-dimensional convolution. After transposing the Sobel filter to extract the vertical edges, both the horizontal and vertical edges were combined to calculate the gradient magnitude of each pixel in the image. Followed by thresholding the gradient magnitude to determine the contours of the area of interest, the gradient orientation was calculated by determining the angle of the gradient with respect to the x-axis.

Gene expression analysis

Following differentiation treatments, as described above, mRNA was isolated from vSMC cultures using the RNAeasy Kit (Qiagen). The cDNA were obtained using the TaqMan cDNA Reverse Transcription Kit (Life Technologies). Real-time polymerase chain reaction (PCR) was performed using the ViiA™ 7 Real-Time PCR System (Applied Biosystems) using a SYBR Green Master Mix (Life Technologies). All PCR results were normalized to the expression levels of GAPDH prior to further analysis. The custom-synthesized primer pairs (Sigma) used for real-time reverse transcription–

PCR are listed in Supplementary Table S1 (Supplementary Data are available online at www.liebertpub.com/tea).

Statistical analysis

All results are shown as mean ± standard error of the mean. A two-tailed Student's *t*-test was used to make comparisons in data with only two groups with $p < 0.05$ counted as statistically significant. ANOVA was used for multiple comparisons and Tukey's *post hoc* testing was used to assess differences between groups. Statistically significant difference between nanopatterned and unpatterned substrata ($p < 0.05$) for the same substratum stiffness is indicated with an asterisk. For all other substrata-type combinations, the identical signage indicates statistically significant difference for that pair.

Results

Nanopatterned and unpatterned PUA substrata with different elastic moduli

The difference in the material properties of the four different fabricated substrata allowed us to investigate the effect of different surface nanotopography and matrix stiffness on vSMC behavior. The Young's modulus was around 11 MPa for the softer substrata and around 1.1 GPa for the stiffer substrata and from now on will be referred to as ''soft'' (for 11 MPa) and ''stiff'' (for 1.1 GPa). SEM and AFM confirmed the presence of nanopatterning with the 800 nm groove dimensions on a large area ($> 1 \times 1$ mm), commensurate with the size scale of individual focal adhesions (~ 1 μm) and scalable to large areas for tissue-scale engineering (Fig. 1B, C). Average groove width and average groove depth were identical for both the soft and stiff ANFS, confirming that the polymer stiffness had no effect on maintaining feature fidelity. Relative to other methods used to create nanopatterned substrata, UV-assisted CFL afforded a way to create the nanopatterning in a fast and cost-effective manner with high pattern fidelity and physical integrity on biocompatible PUA substrata. Our nanopatterning was inspired by the fact that individual collagen fibers tend to have feature sizes around 150 nm, and, therefore, actual collagen fiber bundles that native cells populate have feature sizes of ~ 550–900 nm, varying to some extent in different tissue types.[31] To the best of our knowledge, this is the first study enabling the appreciation of the synergistic effects of altered nanotopography and material elasticity on vSMC behavior.

Analysis of cell elongation and polarization on nanopatterned substrata

Using the mechanically distinct substrata, we analyzed cell shape (Fig. 2A) and alignment relative to the nanogrooves (for the nanopatterned substrata) and relative to the y-axis (for the unpatterned substrata) (Fig. 2B). vSMCs cultured on the nanopatterned substrata were longer (higher EFF) than those cultured on the unpatterned substrata (Fig. 2C). In addition, cell shape appeared to be more sensitive to the nanopatterning on the stiff substrata compared with the soft substrata, with the nanopatterning on the stiff substrata presumably

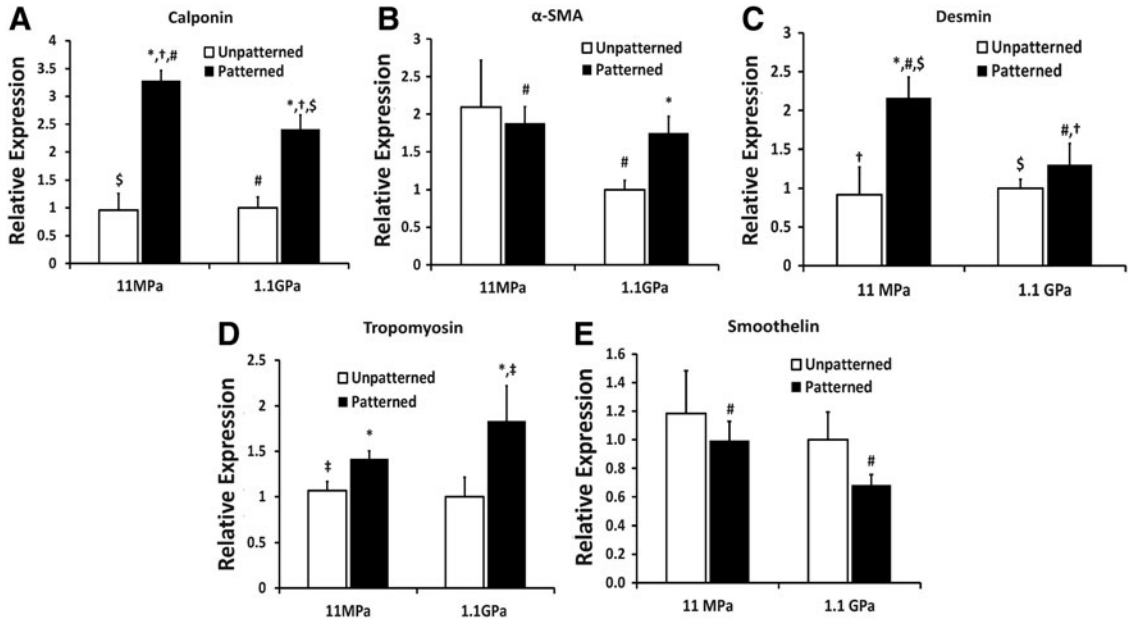

FIG. 3. Real-time polymerase chain reaction (PCR) analyses of various vSMC differentiation-related markers when cultured on the different substrata. Interestingly, for the intermediate filament-related markers calponin and desmin and for the smooth muscle-specific cytoskeletal protein smoothelin, soft ANFS resulted in statistically higher gene expression. This highlights the synergetic effects of substratum nanotopography and elasticity on vSMC differentiation, with ANFS resulting in a more profound effect on vSMC-restricted contractile protein marker genes. Interestingly, for the less stringent marker smooth muscle α-actin (α-SMA) (also found in myofibroblasts), there was no statistical difference between soft and stiff ANFS. For tropomyosin, found to be erratically upregulated in hypertension, stiff ANFS expressed statistically higher levels. Statistically significant difference between nanopatterned and unpatterned substrata ($p < 0.05$) for the same substratum stiffness is indicated with an asterisk. For all other substrata-type combinations, the identical signage indicates statistically significant difference for that pair.

triggering vSMC ''mechanical plasticity.''[27] In contrast, the vSMCs clearly aligned better on the soft substrata with imprinted nanogrooves relative to the stiff substrata.

Analysis of vSMC differentiation on differentially engineered substrata

Since the expression of multiple vSMC-specific differentiation markers can attest to the phenotype of vSMCs, we tested the synergetic effect of engineered nanotopography and stiffness on the gene expression of multiple markers. Nanopatterning the substrata resulted in increase in calponin gene expression, with the expression of calponin being higher in the case of vSMCs cultured on the soft ANFS than on the stiff ANFS (Fig. 3A), highlighting the beneficial effect of physiologically relevant compliance and of nanopatterning the substratum. In addition, nanopatterning the stiff substratum resulted in higher smooth muscle α-actin (α-SMA) gene expression relative to the unpatterned stiff substratum (Fig. 3B), indicating that even in the absence of an optimally stiff substratum, patterning the substratum could enhance vSMC contractility. Further, desmin was also upregulated on the soft ANFS (Fig. 3C), and was significantly lowered on the stiff substratum even when nanopatterned. While desmin is an early marker of muscle cell differentiation, the presence of desmin in vSMCs indicates high functional activity since it links myofibrils to the cell membrane.[32] Desmin has been found greatly diminished in vascular lesions such as in a pig model of directional atherectomy.[33] In addition, the levels of tropomyosin-1 were higher on the nanopatterned substrata relative to the unpatterned substrata (Fig. 3D). While tropomyosin-1 is an established marker for vSMC phenotype, erratic levels of this marker have been associated with hypertension in some tissues.[34] Finally, given that smoothelin is a very sensitive marker for vSMC differentiation,[35] we also tested the synergistic effect of nanopatterning and stiffness on smoothelin gene expression. While the nanopatterning did not statistically alter the expression of smoothelin individually for the unpatterned and patterned substrata, the soft ANFS had statistically higher smoothelin expression relative to the stiff ANFS (Fig. 3E). Since smoothelin has been exclusively found in fully differentiated vSMCs and is absent in myofibroblasts, the upregulation of smoothelin in vSMCs cultured on soft ANFS is particularly interesting. Overall, our findings illustrated the synergetic effect of anisotropic nanopatterning and vascular tissue-like compliance of engineered PUA substrata, with ANFS specifically upregulating the expression of vSMC-restricted contractile protein genes.

Analysis of vSMC activation on the fabricated substrata

Nanopatterning the soft and stiff substrata decreased the gene expression of inflammatory mediators (Fig. 4) such as intercellular adhesion molecule-1 (ICAM-1), tissue factor, and interleukin-6 (IL-6). However, monocyte chemoattractant protein-1 (MCP-1 or CCL2) expression, known to be upregulated in hypertensive individuals,[36] remained high on nanopatterned stiff substrata. This indicated that a stiffer matrix may trigger the homing of inflammatory cells with the activation of the inflammatory NF-κB pathway.[37]

Analysis of the F-actin cytoskeleton of vSMCs on the substrata

The cytoskeletal F-actin stress fibers were clearly different for all four types of substrata (Fig. 5), with the stress

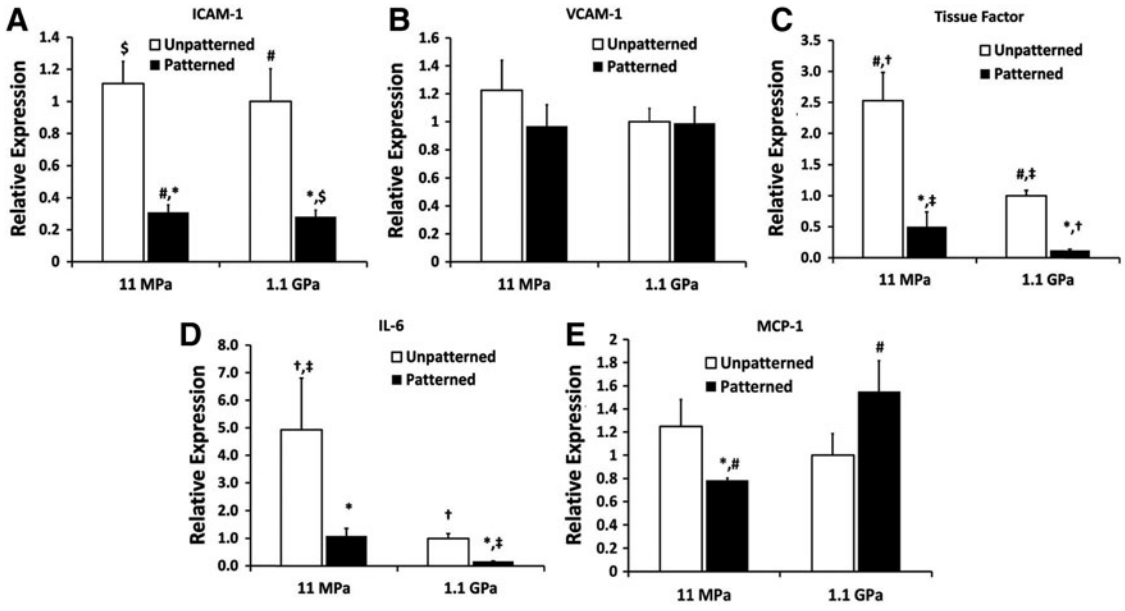

FIG. 4. Real-time PCR analyses of various vSMC-secreted inflammatory markers when cultured on the different substrata. ANFS, for the most part, decreased the gene expression of inflammatory cytokines for both the soft and stiff substrata ($p < 0.05$) and thus made ANFS more biomimetic. Notably, the levels of monocyte chemoattractant protein-1 (MCP-1) expression increased around twofold on stiff ANFS relative to soft ANFS. Statistically significant difference between nanopatterned and unpatterned substrata ($p < 0.05$) for the same substratum stiffness is indicated with an asterisk. For all other substrata-type combinations, the identical signage indicates statistically significant difference for that pair.

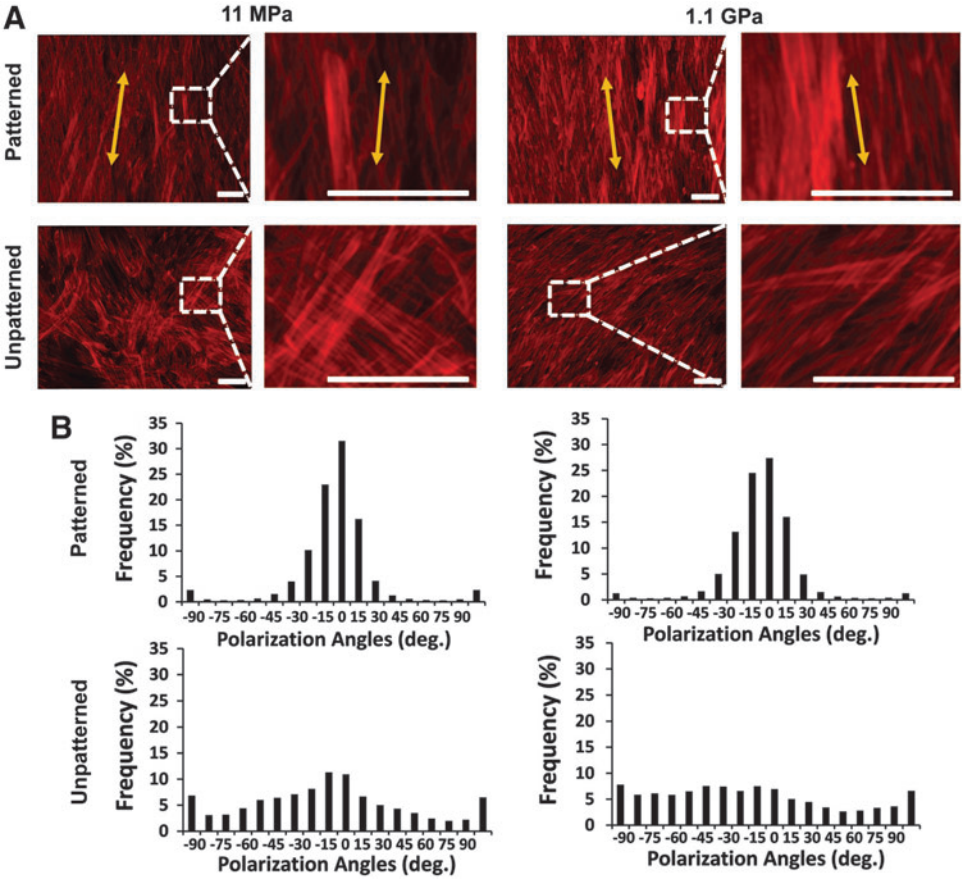

FIG. 5. Altered appearance of the cytoskeletal F-actin stress fibers on the different substrata. **(A)** Immunocytochemical staining of the actin cytoskeleton in vSMCs. Scale bar: 100 μm. **(B)** Clearly, the stress fibers were directionally aligned by both the soft and stiff ANFS, as demonstrated by the histograms.

fibers forming a diffuse meshwork of fibers on the unpatterned substrata. Further, the stress fibers were directionally aligned by the nanopatterning on both soft and stiff substrata and demonstrated a higher intensity on the nanopatterned stiff substrata. Given that the dynamic remodeling of the actin cytoskeleton plays a prominent role in vSMC proliferation and migration,[38] it follows from the altered F-actin cytoskeleton that the different substrata would confer different proliferative and migratory states to the vSMCs.

Potential mechanistic processes involved in cell-sensing of the substratum micromechanics

The Rho pathway has been implicated in the hypercontractility of vSMCs, which could result in vasospasms or hypertension, as reviewed in Refs.[39,40] In addition, the Rho pathway has also been demonstrated to be involved in rigidity sensing and lineage commitment in stem cells.[41] Given that the vSMCs cultured on nanopatterned stiff substrata recapitulated some of the phenotypic characteristics of hypercontractile vSMCs, we explored the components of the Rho-ROCK pathway, specifically RhoA, ROCK1, and ROCK2 gene expression; ROCKs or Rho-associated kinases being the immediate downstream targets of RhoA.[42] As per our prediction, we found statistically higher levels of RhoA, ROCK1, and ROCK2 in the vSMCs cultured on stiff ANFS (Fig. 6A–D). Our hypothesis was based on the fact that vSMCs on stiff ANFS were longer, less circular, and contractile, expressing higher levels of α-SMA, tropomyosin, and F-actin stress fibers, and high levels of the inflammatory cytokine, MCP-1. This points to the possibility that stiffer substrata (such as conventional stents), when ''nanopatterned'' after *in vivo* deployment via the natural deposition of ECM proteins, could potentiate phenotypic switching (triggering mechanical plasticity[27]) of vSMCs, especially in the case of deep medial injury,[43] or, in abnormally reactive smooth muscle tissue phenotype stemming from conditions such as diabetes.[44] This highlights the potential therapeutic benefit of ROCK-inhibitors, such as statins, prior to or post stent deployment. In fact, some of the pleiotropic effects of statins are now attributed to ROCK-inhibition.[45] We also found some of the downstream targets of the Rho-ROCK pathway to be upregulated, the gene expression of which have been well correlated with protein expression and their upregulation has been associated with the hypertensive vSMC phenotype in pulmonary vSMCs[46,47] (Fig. 6E, F). Thus, nanopatterning the stiff substrata appears to alter the Rho-ROCK-LIMK-cofilin pathway in vSMCs, which has been shown to modulate actin assembly in a variety of cell types.[48]

We also found caveolin-1, expressed by plasma membrane invaginations (caveolae) and associated with the differentiated vSMC phenotype,[49] to be significantly upregulated in vSMCs on nanopatterned soft substrata (Fig. 6G). Notably, caveolin-1 suppression has been associated with the proliferative airway smooth muscle phenotype.[50] Of particular relevance to this study is also the fact that caveolin-1 has been shown to confer cell polarity,[51] which makes our finding that caveolin-1 is upregulated in more polarized cells,

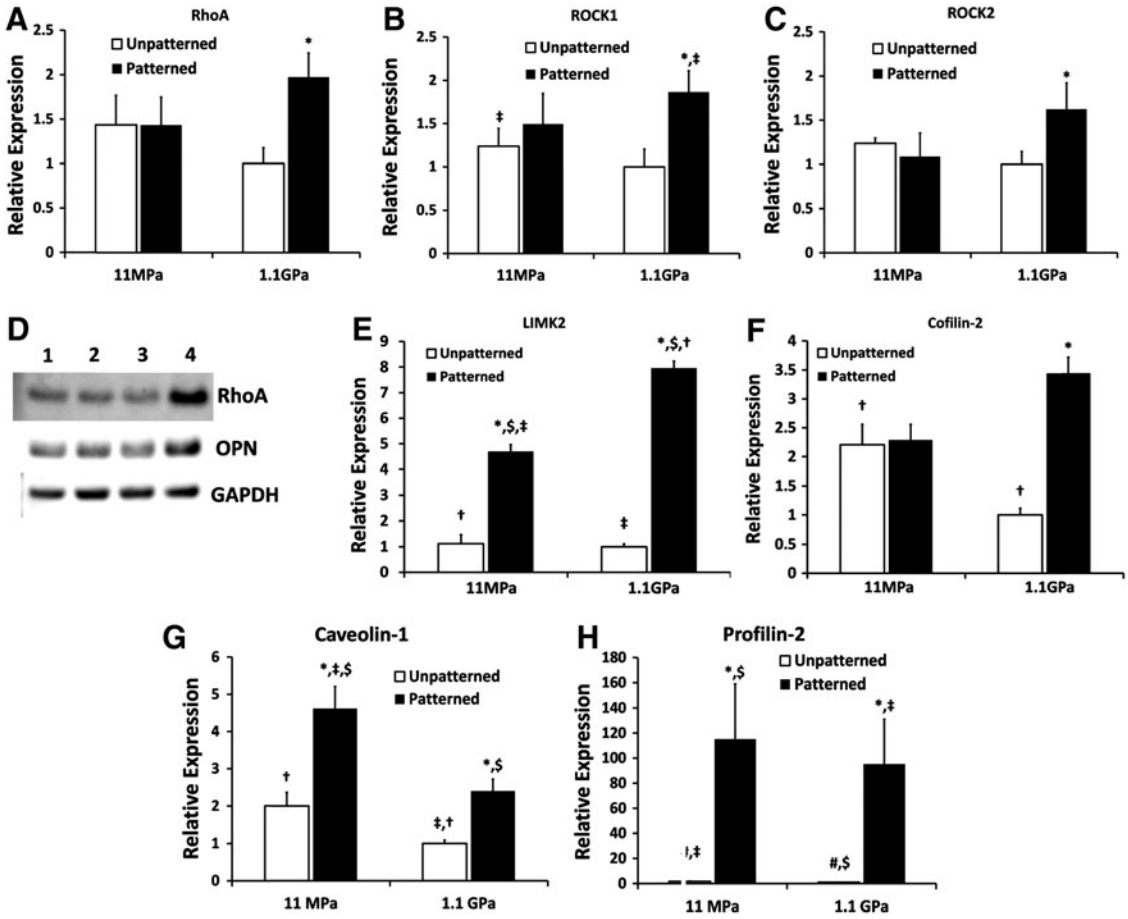

FIG. 6. Altered RhoA-related signaling in vSMCs when cultured on the different substrata. **(A–C)** RhoA upregulation, along with the upregulation of the Rho kinases, ROCK1 and ROCK2, the serine-threonine downstream effectors of RhoA, indicate that the activity of RhoA could be upregulated in the stiff ANFS potentially resulting in overly contractile vSMCs. This phenotype is reminiscent of hypertensive vSMCs and of asthmatic airway smooth muscle cells. **(D)** Western blots for RhoA and osteopontin (OPN) clearly indicated higher levels of RhoA and OPN for stiff ANFS. The order of the blots indicated by *(1–4)* is the same as in the other graphs, that is, *(1)* soft unpatterned, *(2)* soft ANFS, *(3)* stiff unpatterned, and *(4)* stiff ANFS. **(E, F)** LIM kinase 2 (LIMK2) and cofilin-2, both of which are downstream of RhoA, were significantly upregulated in vSMCs on stiff ANFS. Thus, given that the vSMCs on the stiff ANFS are longer (higher EFF), stain higher for F-actin stress fibers, express high levels of α-SMA and tropomyosin, and as seen in **(G)** have lowered levels of caveolin-1, it is probable that the phenotype of the vSMCs on the stiff ANFS is distinct from the others. **(H)** Profilin-2, which has been found to decrease invasiveness and migratory tendencies of cells, was higher in vSMCs cultured on ANFS. Statistically significant difference between nanopatterned and unpatterned substrata ($p < 0.05$) for the same substratum stiffness is indicated with an asterisk. For all other substrata type combinations, the identical signage indicates statistically significant difference for that pair.

specifically those on soft ANFS, interesting. Finally, we also found that the levels of profilin-2 were upregulated in cells on nanopatterned substrata (Fig. 6H), profilin-2 being affiliated to the Rho pathway and capable of suppressing cell motility and invasiveness via an actomyosin contractility-driven mechanism.[52]

Discussion

Cell adhesion to the ECM results in the clustering of cell surface receptors such as integrins and syndecans,[53] creating focal adhesion complexes that can actuate intracellular signaling conduits.[54] Engineering material surfaces that can crosstalk with these focal adhesion complexes at the same level of nanoscale granularity have been demonstrated to influence cell functions and have recently been probed at the single cell level by measuring the traction forces exerted by cells.[55] The blood vessel wall experiences progressive stiffening with age and disease,[56] which alters the micromechanical environment experienced by resident vSMCs forming the bulk of the vessel wall. In addition, the orientation and fibrillar geometry of collagen and elastin are subject to change with altered cardiac and, correspondingly, vascular function,[57] which can be replicated by nanopatterning the substratum. Further, nanopatterning also affords anisotropic elasticity to cultured cells, forcing cells to exert different traction forces along and perpendicular to the direction of the nanogrooves.[58] Here, the dimensions of the topographical features, generally inspired by the sizes of focal complexes, are also of significance. For example, in

our own work, we found that while a 400_400 nm substratum resulted in incomplete cell protrusion into the nanogrooves, an 800_800 nm substratum resulted in more complete protrusion, indicating a more extensive cell–substratum adhesion surface. Further, we found that nanopatterning that was too dense (such as <400 nm) or too sparse (such as >1200 nm) led to situations in which the cell basically saw the substratum as flat.[15] While *in vitro* studies have shown that vSMCs are sensitive to substratum nanotopography[59] and stiffness,[60,61] the synergetic response of matrix architecture and mechanics and the underlying molecular mechanisms modulating altered vSMC mechanotransduction pathways remain unknown.

In this article, we have demonstrated a simple, scalable, and highly reproducible lithographic technique, CFL, which can result in large-area nanopatterning of substrata of varying elastic moduli with high fidelity. Specifically, we demonstrated that altered vSMC phenotypic states can be catalyzed by simultaneously varying the nanotopography and stiffness of the substrata. In particular, nanopatterned substrata resulted in higher expression of vSMC-specific differentiation marker genes especially when the pattern was imprinted on soft substrata forming soft ANFS. Our studies used confluent vSMC densities to simulate a continuous layering of vSMCs and allowed the deposition of serum proteins before cell seeding to mimic the deposition of blood sera on a stent surface, for example, after deployment. In *in vivo* situations, a sub-confluent layer of cells could simulate a breached layer of cells where the cells would initially need to be proliferative. Then, once the voids are filled, these cells would transform to a mature phenotype as in the quiescent smooth muscle. Since the final goal of engineering the substrata would be to be able to integrate the tissue scaffold or device with the surrounding ECM, we were interested in gauging how the substratum could alter the phenotype of the vSMCs and result in altered inflammatory signatures in wound healing-like situations. Thus, we probed the inflammatory cytokines and cell adhesion markers (CAMs) expressed by vSMCs on the different substrata. Interestingly, while there was no statistical alteration in VCAM-1, ICAM-1 expression was significantly lower in vSMCs on soft and stiff ANFS. It has been demonstrated that ICAM-1 and VCAM-1 are both inducible in vSMCs by different inflammatory stimuli. For example, different inflammatory cytokines can invoke the increase in these CAMs differentially, potentially eliciting varied inflammatory signaling cascades.[62] Overall, it was clear that nanopatterning the substrata decreased inflammatory signals, other than MCP-1; the latter remained elevated even after nanopatterning the stiff substratum.

In conclusion, our data point to the ability of a soft ANFS to diminish the inflammatory response and facilitate vSMC differentiation upon implantation, as summarized in Figure 7. The implantation of a vascular scaffold, especially with matrix-embedded vascular cells has been found to have marked therapeutic potential in the case of vascular

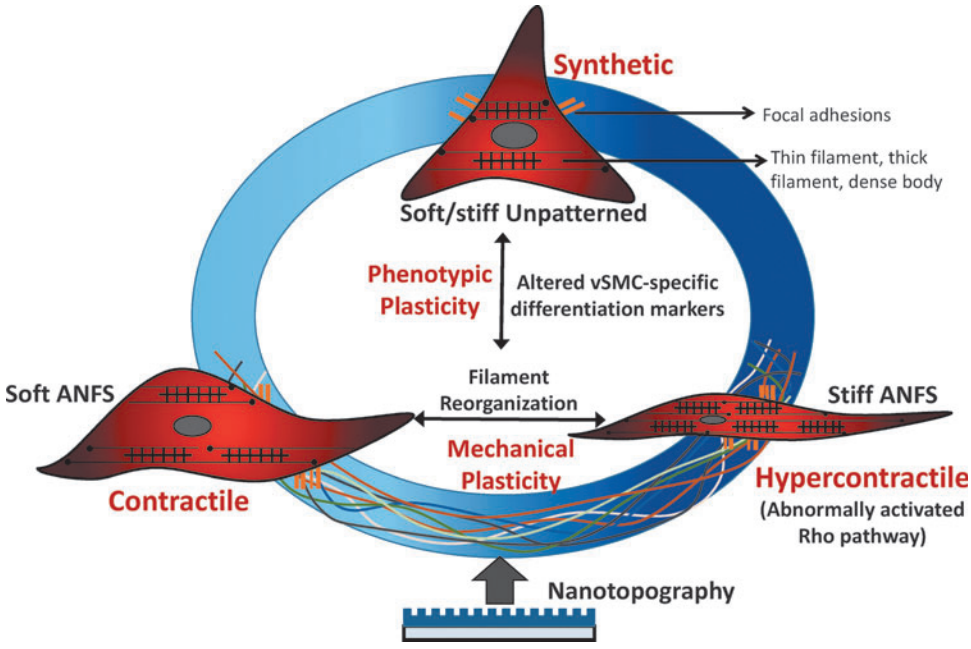

FIG. 7. The phenotypic continuum demonstrated by vSMCs can be thought of as a function of both cytoskeletal remodeling (mechanical plasticity) and altered expression of vSMC-specific marker genes (phenotypic plasticity). The schematic presented here depicts the ability of matrix nanotopography (simulating matrix fibrils such as collagen and elastin) and stiffness (simulating the packing of the extracellular matrix proteins) to potentiate changes in smooth muscle function characterized by the more traditional, synthetic (proliferative), and contractile (mature differentiated) phenotypes, and the third, often overlooked, hypercontractile phenotype. Results presented in this study alluded to the possibility of conferring such a hypercontractile phenotype to the muscle cells when cultured on a stiff ANFS. This could be triggered by abnormal levels of Rho pathway effectors and cause diseased states found in hypertension or type II diabetes. ANFS refers to our ANFS using CFL.

lesions.[63] In such cases, our soft ANFS may be better poised to be a material of choice. Further, in the case of stenting devices that are known to trigger vascular lesions[64] and call upon the use of stiffer substrata for affording structural support, engineering the surface nanotopography can potentially improve the clinical outcomes. In this regard, CFL may pave the way to test a combinatorial library of nanopattern arrays with different topographical parameters to determine the best-suited topography for the desired outcome. In wound healing after vascular interventions, it may also be desirable to have a graded continuum of varying density of topographic features on the implant, as demonstrated in our innovative study using fibroblasts to mimic matrix remodeling in wound repair,[17] the spacing in the topographic features being determined by factors such as fluid flow dynamics[65] and the degree of plaque or thrombus formation[66] at the site of intervention. Finally, the higher expression of RhoA and downstream RhoA effectors by vSMCs cultured on stiff ANFS allude to the possibility that implants made of stiffer materials may drive vSMCs toward a hypercontractile phenotype. Such situations may not only call for the administration of ROCK-inhibitors[67] but also, in the first place, to engineer the nanotopography of the scaffold or device preventing or diminishing undesirable cell–substratum interactions.

Collectively, this study provides insight into the mechanisms by which vSMCs respond to the matrix-modulated mechanical environment, recapitulating the architecture of the basement membrane underlying the smooth muscle layers. It also points to the importance of controlled topographical and micromechanical cues in vascular mechanotransduction studies. This study further presents a simple reproducible method to alter the nanotopography of the substrata using CFL that can be exploited to mimic nanostructural changes in collagen or elastin fibril architecture in disease, aging, or vascular remodeling.

Acknowledgments

D.-H.K. thanks the Department of Bioengineering at the University of Washington for the new faculty startup fund. This work was also supported by the American Heart Association Scientist Development Grant 13SDG14560076 (to D.-H.K.), the American Heart Association Scientist Development Grant 10SDG2630139 (to A.B.B.), and the National Institutes of Health grant 1DP2OD008716-01 (to A.B.B.). The authors thank Peter Kim and Kevin Mun for their technical assistance to conduct the atomic force microscopy.

Disclosure Statement

No competing financial interests exist.

References

1. Cordes, K.R., Sheehy, N.T., White, M.P., Berry, E.C., Morton, S.U., Muth, A.N., *et al.* miR-145 and miR-143 regulate smooth muscle cell fate and plasticity. Nature **460,** 705, 2009.
2. McDonald, O.G., and Owens, G.K. Programming smooth muscle plasticity with chromatin dynamics. Circ Res **100,** 1428, 2007.
3. Miano, J.M. Deck of CArGs. Circ Res **103,** 13, 2008.
4. O'Connell, M.K., Murthy, S., Phan, S., Xu, C., Buchanan, J., Spilker, R., *et al.* The three-dimensional micro-and nanostructure of the aortic medial lamellar unit measured using 3D confocal and electron microscopy imaging. Matrix Biol **27,** 171, 2008.
5. Timmins, L.H., Wu, Q., Yeh, A.T., Moore, J.E., and Greenwald, S.E. Structural inhomogeneity and fiber orientation in the inner arterial media. Am J Physiol Heart Circ Physiol **298,** H1537, 2010.
6. Yu, J., Tirlapur, U., Fairbank, J., Handford, P., Roberts, S., Winlove, C.P., *et al.* Microfibrils, elastin fibres and collagen fibres in the human intervertebral disc and bovine tail disc. J Anat **210,** 460, 2007.
7. Kim, D.-H., Provenzano, P.P., Smith, C.L., and Levchenko, A. Matrix nanotopography as a regulator of cell function. J Cell Biol **197,** 351, 2012.
8. Chalut, K.J., Kulangara, K., Giacomelli, M.G., Wax, A., and Leong, K.W. Deformation of stem cell nuclei by nanotopographical cues. Soft Matter **6,** 1675, 2010.
9. Xu, C., Inai, R., Kotaki, M., and Ramakrishna, S. Electrospun nanofiber fabrication as synthetic extracellular matrix and its potential for vascular tissue engineering. Tissue Eng **10,** 1160, 2004.
10. Liliensiek, S.J., Nealey, P., and Murphy, C.J. Characterization of endothelial basement membrane nanotopography in rhesus macaque as a guide for vessel tissue engineering. Tissue Eng Part A **15,** 2643, 2009.
11. Bettinger, C.J., Langer, R., and Borenstein, J.T. Engineering substrate topography at the micro- and nanoscale to control cell function. Angew Chem Int Ed Engl **48,** 5406, 2009.
12. Malmström, J., Christensen, B., Jakobsen, H.P., Lovmand, J., Foldbjerg, R., Sørensen, E.S., *et al.* Large area protein patterning reveals nanoscale control of focal adhesion development. Nano Lett **10,** 686, 2010.
13. Beningo, K.A., Dembo, M., Kaverina, I., Small, J.V., and Wang, Y.-L. Nascent focal adhesions are responsible for the generation of strong propulsive forces in migrating fibroblasts. J Cell Biol **153,** 881, 2001.
14. Geiger, B., Spatz, J.P., and Bershadsky, A.D. Environmental sensing through focal adhesions. Nat Rev Mol Cell Biol **10,** 21, 2009.
15. Kim, D.-H., Lipke, E.A., Kim, P., Cheong, R., Thompson, S., Delannoy, M., *et al.* Nanoscale cues regulate the structure and function of macroscopic cardiac tissue constructs. Proc Natl Acad Sci U S A **107,** 565, 2010.
16. Costa, K.D., Lee, E.J., and Holmes, J.W. Creating alignment and anisotropy in engineered heart tissue: role of boundary conditions in a model three-dimensional culture system. Tissue Eng **9,** 567, 2003.
17. Kim, D.-H., Han, K., Gupta, K., Kwon, K.W., Suh, K.-Y., and Levchenko, A. Mechanosensitivity of fibroblast cell shape and movement to anisotropic substratum topography gradients. Biomaterials **30,** 5433, 2009.
18. Kim, D.H., Seo, C.H., Han, K., Kwon, K.W., Levchenko, A., and Suh, K.Y. Guided cell migration on microtextured substrates with variable local density and anisotropy. Adv Funct Mater **19,** 1579, 2009.
19. Yang, Y., Kulangara, K., Sia, J., Wang, L., and Leong, K.W. Engineering of a microfluidic cell culture platform embedded with nanoscale features. Lab Chip **11,** 1638, 2011.
20. Wang, B., Weldon, A.L., Kumnorkaew, P., Xu, B., Gilchrist, J.F., and Cheng, X. Effect of surface nanotopography on immunoaffinity cell capture in microfluidic devices. Langmuir **27,** 11229, 2011.

21. Frohlich, E., Alonso, J.L., Zhang, X., Borenstein, J., Arnaout, M.A., and Charest, J.L. Topographically-patterned porous membranes in a microfluidic device as an *in vitro* model of renal reabsorptive barriers. Lab Chip **13,** 2311, 2013.
22. Kilian, K.A., Bugarija, B., Lahn, B.T., and Mrksich, M. Geometric cues for directing the differentiation of mesenchymal stem cells. Proc Natl Acad Sci U S A **107,** 4872, 2010.
23. Nemir, S., and West, J.L. Synthetic materials in the study of cell response to substrate rigidity. Ann Biomed Eng **38,** 2, 2010.
24. Gordan, O.D., Persson, B.N.J., Cesa, C.M., Mayer, D., Hoffmann, B., Dieluweit, S., *et al.* On pattern transfer in replica molding. Langmuir **24,** 6636, 2008.
25. Akhtar, R., Schwarzer, N., Sherratt, M., Watson, R., Graham, H., Trafford, A., *et al.* Nanoindentation of histological specimens: mapping the elastic properties of soft tissues. J Mater Res **24,** 638, 2009.
26. Orr, A.W., Hastings, N.E., Blackman, B.R., and Wamhoff, B.R. Complex regulation and function of the inflammatory smooth muscle cell phenotype in atherosclerosis. J Vasc Res **47,** 168, 2009.
27. Halayko, A.J., and Solway, J. Invited review: molecular mechanisms of phenotypic plasticity in smooth muscle cells. J Appl Physiol **90,** 358, 2001.
28. Sazonova, O.V., Lee, K.L., Isenberg, B.C., Rich, C.B., Nugent, M.A., and Wong, J.Y. Cell-cell interactions mediate the response of vascular smooth muscle cells to substrate stiffness. Biophys J **101,** 622, 2011.
29. Chaterji, S., Park, K., and Panitch, A. Scaffold-free *in vitro* arterial mimetics: the importance of smooth muscle–endothelium contact. Tissue Eng Part A **16,** 1901, 2010.
30. Cho, H., Jönsson, H., Campbell, K., Melke, P., Williams, J.W., Jedynak, B., *et al.* Self-organization in high-density bacterial colonies: efficient crowd control. PLoS Biol **5,** e302, 2007.
31. Perumal, S., Antipova, O., and Orgel, J.P.R.O. Collagen fibril architecture, domain organization, and triple-helical conformation govern its proteolysis. Proc Natl Acad Sci U S A **105,** 2824, 2008.
32. Mericskay, M., Parlakian, A., Porteu, A., Dandré, F., Bonnet, J., Paulin, D., *et al.* An overlapping CArG/octamer element is required for regulation of desmin gene transcription in arterial smooth muscle cells. Dev Biol **226,** 192, 2000.
33. Gonschior, P., Gerheuser, F., Gonschior, G.-M., Maier, G.R., Mack, B., Nerlich, A., *et al.* Experimental directional atherectomy injury in arterial vessels: impact of trauma depth on cellular response. Am Heart J **129,** 1067, 1995.
34. Dunn, S.A., Mohteshamzadeh, M., Daly, A.K., and Thomas, T.H. Altered tropomyosin expression in essential hypertension. Hypertension **41,** 347, 2003.
35. van der Loop, F.T., Gabbiani, G., Kohnen, G., Ramaekers, F.C., and van Eys, G.J. Differentiation of smooth muscle cells in human blood vessels as defined by smoothelin, a novel marker for the contractile phenotype. Arterioscler Thromb Vasc Biol **17,** 665, 1997.
36. Egashira, K. Molecular mechanisms mediating inflammation in vascular disease: special reference to monocyte chemoattractant protein-1. Hypertension **41,** 834, 2003.
37. Weber, K.T. From inflammation to fibrosis: a stiff stretch of highway. Hypertension **43,** 716, 2004.
38. Kim, H.R., Gallant, C., Leavis, P.C., Gunst, S.J., and Morgan, K.G. Cytoskeletal remodeling in differentiated vascular smooth muscle is actin isoform dependent and stimulus dependent. Am J Physiol Cell Physiol **295,** C768, 2008.
39. Fukata, Y., Amano, M., and Kaibuchi, K. Rho-Rho-kinase pathway in smooth muscle contraction and cytoskeletal reorganization of non-muscle cells. Trends Pharmacol Sci **22,** 32, 2001.
40. Loirand, G., Guérin, P., and Pacaud, P. Rho kinases in cardiovascular physiology and pathophysiology. Circ Res **98,** 322, 2006.
41. McBeath, R., Pirone, D.M., Nelson, C.M., Bhadriraju, K., and Chen, C.S. Cell shape, cytoskeletal tension, and RhoA regulate stem cell lineage commitment. Dev Cell **6,** 483, 2004.
42. Noma, K., Oyama, N., and Liao, J.K. Physiological role of ROCKs in the cardiovascular system. Am J Physiol Cell Physiol **290,** C661, 2006.
43. Gunn, J., Arnold, N., Chan, K., Shepherd, L., Cumberland, D., and Crossman, D. Coronary artery stretch versus deep injury in the development of in-stent neointima. Heart **88,** 401, 2002.
44. Xie, Z., Gong, M.C., Su, W., Xie, D., Turk, J., and Guo, Z. Role of calcium-independent phospholipase a2β in high glucose-induced activation of RhoA, Rho kinase, and CPI-17 in cultured vascular smooth muscle cells and vascular smooth muscle hypercontractility in diabetic animals. J Biol Chem **285,** 8628, 2010.
45. Nohria, A., Prsic, A., Liu, P.-Y., Okamoto, R., Creager, M.A., Selwyn, A., *et al.* Statins inhibit Rho kinase activity in patients with atherosclerosis. Atherosclerosis **205,** 517, 2009.
46. Bongalon, S., Dai, Y.P., Singer, C.A., and Yamboliev, I.A. PDGF and IL-1β upregulate cofilin and LIMK2 in canine cultured pulmonary artery smooth muscle cells. J Vasc Res **41,** 412, 2004.
47. Dai, Y.-P., Bongalon, S., Tian, H., Parks, S.D., Mutafova-Yambolieva, V.N., and Yamboliev, I.A. Upregulation of profilin, cofilin-2 and LIMK2 in cultured pulmonary artery smooth muscle cells and in pulmonary arteries of monocrotaline-treated rats. Vasc Pharmacol **44,** 275, 2006.
48. Lin, T., Zeng, L., Liu, Y., DeFea, K., Schwartz, M.A., Chien, S., *et al.* Rho-ROCK-LIMK-cofilin pathway regulates shear stress activation of sterol regulatory element binding proteins. Circ Res **92,** 1296, 2003.
49. Hardin, C.D., and Vallejo, J. Caveolins in vascular smooth muscle: form organizing function. Cardiovasc Res **69,** 808, 2006.
50. Aravamudan, B., VanOosten, S.K., Meuchel, L.W., Vohra, P., Thompson, M., Sieck, G.C., *et al.* Caveolin-1 knockout mice exhibit airway hyperreactivity. Am J Physiol Lung Cell Mol Physiol **303,** L669, 2012.
51. Grande-García, A., Echarri, A., de Rooij, J., Alderson, N.B., Waterman-Storer, C.M., Valdivielso, J.M., *et al.* Caveolin-1 regulates cell polarization and directional migration through Src kinase and Rho GTPases. J Cell Biol **177,** 683, 2007.
52. Mouneimne, G., Hansen, S.D., Selfors, L.M., Petrak, L., Hickey, M.M., Gallegos, L.L., *et al.* Differential remodeling of actin cytoskeleton architecture by profilin isoforms leads to distinct effects on cell migration and invasion. Cancer Cell **22,** 615, 2012.
53. Morgan, M.R., Humphries, M.J., and Bass, M.D. Synergistic control of cell adhesion by integrins and syndecans. Nat Rev Mol Cell Biol **8,** 957, 2007.

54. Parsons, J.T., Horwitz, A.R., and Schwartz, M.A. Cell adhesion: integrating cytoskeletal dynamics and cellular tension. Nat Rev Mol Cell Biol **11,** 633, 2010.
55. Legant, W.R., Choi, C.K., Miller, J.S., Shao, L., Gao, L., Betzig, E., *et al.* Multidimensional traction force microscopy reveals out-of-plane rotational moments about focal adhesions. Proc Natl Acad Sci U S A **110,** 881, 2013.
56. Qiu, H., Zhu, Y., Sun, Z., Trzeciakowski, J.P., Gansner, M., Depre, C., *et al.* Short communication: vascular smooth muscle cell stiffness as a mechanism for increased aortic stiffness with aging. Circ Res **107,** 615, 2010.
57. Baicu, C.F., Stroud, J.D., Livesay, V.A., Hapke, E., Holder, J., Spinale, F.G., *et al.* Changes in extracellular collagen matrix alter myocardial systolic performance. Am J Physiol Heart Circ Physiol **284,** H122, 2003.
58. Yim, E.K., Darling, E.M., Kulangara, K., Guilak, F., and Leong, K.W. Nanotopography-induced changes in focal adhesions, cytoskeletal organization, and mechanical properties of human mesenchymal stem cells. Biomaterials **31,** 1299, 2010.
59. Yim, E.K., Reano, R.M., Pang, S.W., Yee, A.F., Chen, C.S., and Leong, K.W. Nanopattern-induced changes in morphology and motility of smooth muscle cells. Biomaterials **26,** 5405, 2005.
60. Isenberg, B.C., DiMilla, P.A., Walker, M., Kim, S., and Wong, J.Y. Vascular smooth muscle cell durotaxis depends on substrate stiffness gradient strength. Biophys J **97,** 1313, 2009.
61. Peyton, S.R., and Putnam, A.J. Extracellular matrix rigidity governs smooth muscle cell motility in a biphasic fashion. J Cell Physiol **204,** 198, 2005.
62. Bishop-Bailey, D., Burke-Gaffney, A., Hellewell, P.G., Pepper, J.R., and Mitchell, J.A. Cyclo-oxygenase-2 regulates inducible ICAM-1 and VCAM-1 expression in human vascular smooth muscle cells. Biochem Biophys Res Commun **249,** 44, 1998.
63. Indolfi, L., Baker, A.B., and Edelman, E.R. The role of scaffold microarchitecture in engineering endothelial cell immunomodulation. Biomaterials **33,** 7019, 2012.
64. Inoue, T., Uchida, T., Yaguchi, I., Sakai, Y., Takayanagi, K., and Morooka, S. Stent-induced expression and activation of the leukocyte integrin Mac-1 is associated with neointimal thickening and restenosis. Circulation **107,** 1757, 2003.
65. LaDisa, J., Jr., Guler, I., Olson, L., Hettrick, D., Kersten, J., Warltier, D., *et al.* Three-dimensional computational fluid dynamics modeling of alterations in coronary wall shear stress produced by stent implantation. Ann Biomed Eng **31,** 972, 2003.
66. Hwang, C.-W., Levin, A.D., Jonas, M., Li, P.H., and Edelman, E.R. Thrombosis modulates arterial drug distribution for drug-eluting stents. Circulation **111,** 1619, 2005.
67. Rikitake, Y., and Liao, J.K. Rho GTPases, statins, and nitric oxide. Circ Res **97,** 1232, 2005.

Address correspondence to:
Deok-Ho Kim, PhD
Department of Bioengineering
University of Washington
Box 355061
Seattle, WA 98195

E-mail: deokho@uw.edu

Aaron B. Baker, PhD
Department of Biomedical Engineering
Cockrell School of Engineering
The University of Texas at Austin
1 University Station
BME 5.202D, MC C0800
Austin, TX 78712

E-mail: abbaker@austin.utexas.edu

Received: July 26, 2013
Accepted: January 22, 2014
Online Publication Date: April 1, 2014